optica

Ultracompact metasurface in-line polarimeter

J. P. Balthasar Mueller,[1] Kristjan Leosson,[2,3] and Federico Capasso[1,*]

[1]Harvard School of Engineering and Applied Science, Cambridge, Massachusetts 02138, USA
[2]Innovation Center, Reykjavik, Iceland
[3]Science Institute, University of Iceland, Reykjavik, Iceland
*Corresponding author: capasso@seas.harvard.edu

In-line polarimeters perform nondestructive polarization measurements of optical signals, and play a critical role in monitoring and controlling the polarization environment in, for example, optical networks. While current in-line polarimeters are constructed with multiple optical components, either fabricated into an optical fiber or using free-space optics, we present here a novel architecture conducive to monolithic on-chip integration. This enables the scalable fabrication of high-performance polarization sensors with exceptional stability, compactness, and speed. The method relies on the detection of the highly polarization-dependent scattered field of a subwavelength antenna array known as a metasurface, and is shown here to provide polarization state measurements matching those of a state-of-the-art commercial polarimeter.   © 2016 Optical Society of America

1. INTRODUCTION

Polarization characterizes the vectorial nature of electromagnetic (EM) radiation, which represents a fundamental property separate from its frequency and intensity. The measurement of polarization reveals rich information about, for example, the structure and composition of materials [1], the handedness of chiral molecules [2], and generally about the nature of scattering, emission, and absorption phenomena [3–6]. Polarization can, for example, be used to ascertain the texture and orientation of surfaces in remote sensing applications, and help defeat fog, camouflage, and image clutter [7]. It also represents an important control parameter in engineering light–matter interactions, including in waveguiding [8–13], nanofabrication [14,15], and biomedicine [16]. Several widely employed characterization techniques rely primarily on polarization measurements, such as ellipsometry and chiral sensing [17,18]. Polarization sensitivity is also used to substantially enhance the functionality of optical and radiofrequency technologies, such as in polarization spectroscopy, microscopy, imaging, and radar systems. Unchecked polarization effects can substantially impair network performance in optical telecommunications, which calls for expansive polarization monitoring as the demand for bandwidth rises [19,20]. At the same time, polarization can also be used to improve network bandwidth in polarization diverse systems, and it plays a central role in nascent quantum information technology [21–23]. Despite this vast technological potential, polarization is nevertheless seldom measured, compared to, for example, intensity or frequency. This may in part be explained by the difficulty associated with capturing its inherently vectorial nature: polarization measurements require several measurements of the same signal, each targeting one of its vector components. This issue is addressed by current polarimeters by dividing the signal up either in space or in time [7,24]. Typically, the signal is either split into several beam paths (amplitude division), spread over an array of analyzers (wavefront division), or measured multiple times with a time-varying analyzer (time division). Consequently, polarimeters based on conventional discrete optical components quickly grow too large or expensive for many applications, such as the monitoring of thousands of fiber links or *in vivo* polarization sensing. Frequently, the need for a birefringent medium to measure polarization helicity can additionally drive up the minimum cost and size of polarimeters, and suitable materials are not readily available for all wavelength ranges.

Nanophotonics research has in recent years demonstrated ultracompact optical components based on planar subwavelength structures that are capable of engineering the phase front of reflected and/or refracted light. Such "metasurfaces" can mimic bulk optics, but also achieve new functionality [25]. The latter notably includes the ability to reduce an entire system of bulk optical components to a single, ultrathin optical element, such as achromats [26] and high-NA aspheres [27]. The flexibility in tuning metasurface functionality through their structure can also bypass the reliance on special material properties, such as birefringence [15,28]. Metasurfaces consequently represent an opportunity for polarimetry to overcome unwieldy and expensive architectures [29–36], but implementations so far have suffered from parasitic losses, low efficiency, or a need for digital data processing. Some designs also partially negate the size advantage of metasurfaces by requiring detection of light in the far field. We demonstrate in this article a polarimeter that benefits from the flexibility, simplicity,

and extreme compactness of a metasurface without introducing such drawbacks. Our design deliberately avoids the use of surface plasmon propagation to minimize optical losses, and relies instead on highly directional scattering to directly measure the state of polarization (SOP).

Practical polarimeter designs generally fall into one of two categories: either the entire signal is partially filtered, e.g., by rotating polarizers, and the remaining intensity is fully converted into photocurrent (destructive measurement), or small fractions of the incoming signal are selectively split off for polarization measurement, leaving the original signal largely unperturbed (nondestructive measurement). Nondestructive, or "in-line," polarimeters are needed for, for example, feedback-driven polarization generation, or when a signal must be monitored live without absorbing it, such as in optical networking. The polarimeter we introduce here performs nondestructive measurements upon transmission through a 2D array of subwavelength antennas, capitalizing on the weak scattering of the antennas to minimize perturbation of the signal.

Conventional in-line polarimeters may use partially transmissive mirrors [37] [Fig. 1(a)]. These polarimeters measure the components of the polarization vector through amplitude division by sampling the signal multiple times as it propagates through the polarimeter. Each time, a different polarization component is filtered using polarization optics, and measured using photodetectors. Fiber-based in-line polarimeters, which represent the most common form of in-line polarimeters, may use two tilted fiber Bragg gratings separated by a fiber equivalent of a $\lambda/4$ wave plate to split off fractions of the propagating signal [Fig. 1(b)]. Neither design generally preserves the polarization of the incident beam.

2. CONCEPT

In contrast to existing architectures, the in-line polarimeter presented here relies on only a single, ultrathin optical element [Fig. 1(c)]. The element, consisting of a 2D metasurface, causes highly polarization-selective directional scattering of the signal as it is transmitted through the polarimeter. The polarization information can then be deduced by directly measuring the intensity of the scattered field at a number of discrete points in space, requiring no polarization filtering. Crucially, the scattered field can be sampled co-planar and very close to the metasurface, which distinguishes it from designs that rely on the far-field detection of diffraction orders. This facilitates dense, planar integration that fully capitalizes on the compactness of the metasurface approach. The design of the antenna arrangement is based on straightforward and intuitive design rules, rather than complex numerical modeling, and can be adapted to a different wavelength range through simple scaling.

The polarization state of electromagnetic waves is historically described using a four-element column vector containing the Stokes parameters $\mathbf{S} = (S_0, S_1, S_2, S_3)^T$, where superscript T denotes the matrix transpose [1,19,38,39]. This may be rewritten $S = (I, pIs_1, pIs_2, pIs_3)^T$, where I is the intensity of the wave; $p \in [0, 1]$ its degree of polarization (DOP); and s_1, s_2, and s_3 are the components of a 3D unit vector $\mathbf{s} = \hat{\mathbf{s}}_1 s_1 + \hat{\mathbf{s}}_2 s_2 + \hat{\mathbf{s}}_3 s_3$ that characterizes the SOP of the wave. Through the description as a unit vector, all possible SOPs may be geometrically represented as a point on a unit sphere called a Poincaré sphere [Fig. 2(a)]. A polarimeter generally functions by performing n independent
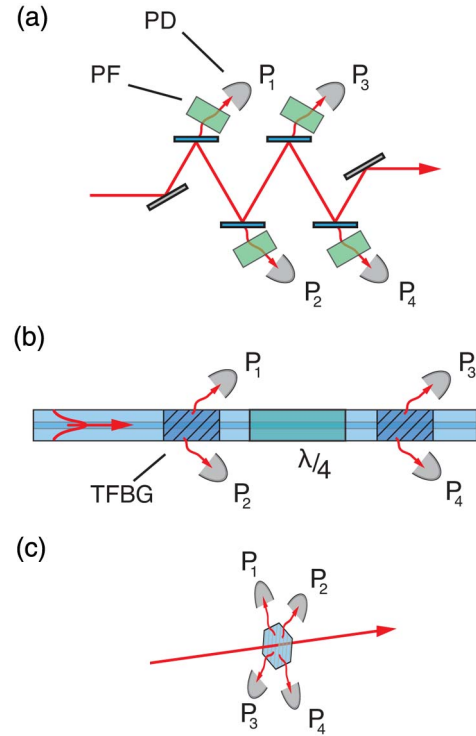

Fig. 1. In-line polarimeter architectures. (a) In-line polarimeter architecture based on discrete optical components. The signal (red) is reflected off several semitransparent mirrors, each time transmitting a fraction of the signal. Different polarization components are measured by applying different polarization filters (PFs) to the transmitted intensities and measuring them with photodetectors (PDs). (b) Fiber-based in-line polarimeter as used in optical networking. Tilted fiber Bragg gratings (TFBGs) act as polarization beam splitters, coupling out beams corresponding to two different polarization components of the signal. Measuring the beams scattered by two TFBGs separated by a fiber wave plate yields sufficient information for determining the polarization state in the fiber. (c) A subwavelength antenna array can be engineered to generate four (or more) scattered beams, related in intensity to different polarization components of the incident signal. Fast polarization measurements are possible by directly detecting those beams, resulting in an extremely compact architecture with a single, essentially two-dimensional, optical element and four (or more) photodetectors.

optical power measurements $P_1, P_2, \ldots P_n$ corresponding to projective measurements of the Stokes vector of the signal $\mathbf{S}$. Assuming a linear response, the set of power measurements is related to the Stokes vector of the signal $\mathbf{S}$ through an $n \times 4$ device matrix $\mathbf{M}$ as $\mathbf{P} = \mathbf{MS}$, where $\mathbf{P} = (P_1, P_2, \ldots P_n)^T$. Each row of the matrix $\mathbf{M}$ then corresponds to the Stokes vector of a polarization component that is sampled by the polarimeter. The polarization state is determined from the power measurements by inverting the device matrix, via $\mathbf{S} = \mathbf{M}^{-1}\mathbf{P}$. The accuracy and extent to which polarization can be deduced depends on the properties of the device matrix with respect to inversion, and the left inverse of the device matrix, $\tilde{\mathbf{M}}^{-1} = (\mathbf{M}^T\mathbf{M})^{-1}\mathbf{M}^T$, can be used instead of $\mathbf{M}^{-1}$ when the dimensions of $\mathbf{M}$ are not 4×4 [24]. The optimization of the device matrix is a problem that is generally applicable to polarimeter design, not just the architecture discussed here, and is discussed in greater detail in Supplement 1, Section 4, which discusses device matrix design. An excellent treatment can be found in Ref. [39]. For the purpose of the
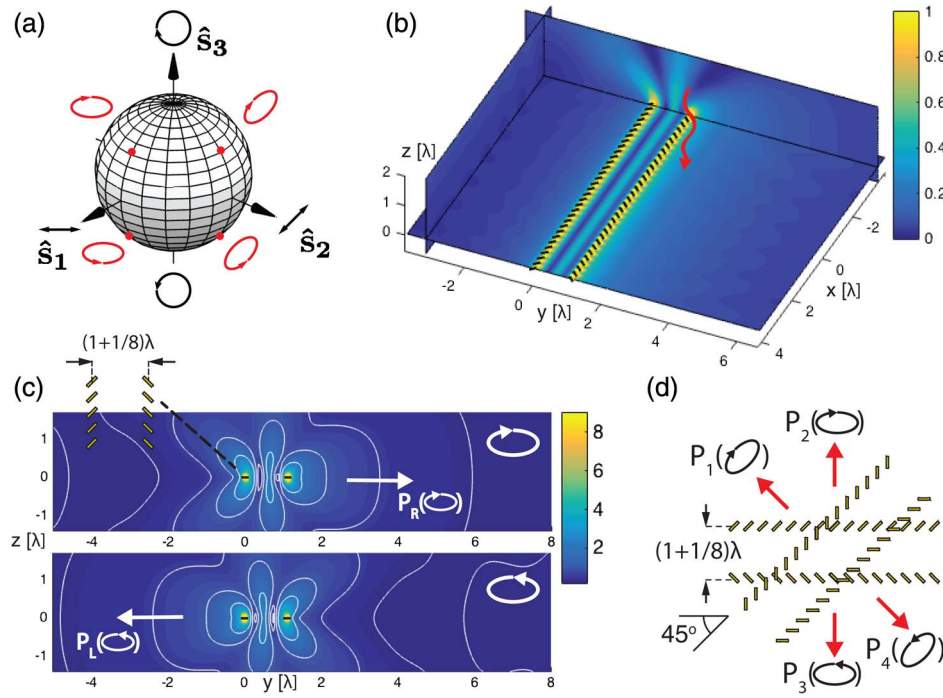
Fig. 2. Polarization-selective directional scattering. (a) The Poincaré sphere representation of state of polarization as a point on the unit sphere. The four elliptical polarization components directionally scattered by the antenna array are shown in red. Measuring these components unambiguously defines the state of polarization of a polarized signal. Note that orthogonal polarization states correspond to diametrically opposite points on the sphere. (b) Illuminated at normal incidence, two parallel rows of subwavelength antennas with $\pm45°$ orientation with respect to the row axis emit a radiation field that is homogeneous along the axes of the rows, but polarization dependent in its radial distribution. The field intensity is here calculated by approximating the antennas as perfect noninteracting dipoles, and is shown on a color scale in arbitrary units. (c) When the rows are laterally displaced by $(1 + 1/8)\lambda$, the row pair directionally scatters elliptically polarized light, with the direction depending on the handedness of the incident polarization. The field intensity is here calculated as in (c) and shown in arbitrary units. (d) Two such pairs of rows superimposed at a $45°$ relative angle result in polarization-selective directional scattering of the desired four elliptical polarization states marked in (a).

current study, we are interested in measuring the SOP of light directly at the end facet of a single-mode optical fiber, illustrating the exceptional compactness of our polarimeter design, and its application to the technologically relevant problem of in-line SOP monitoring in fiber-based telecommunications. The antenna array is designed such that it scatters a small part of the normally incident signal directionally in four different directions co-planar with the array, with the intensity scattered in each of the directions proportional to the strength of a different polarization component. The respective measurements $P_1, ..., P_4$ are then made by detecting the power propagating into each direction, and the linear relationship of these values to the incident polarization state **S** gives the instrument matrix of the polarimeter **M**. In order for the inversion of **M** to allow for the complete determination of the SOP, the four scattered polarization components need to form a basis for the SOP space. That is, the set of power measurements must uniquely determine the signal SOP vector. A particular difficulty lies here in making the structure sensitive to polarization helicity (the $\hat{s}_3$ component). This issue was recently addressed in the context of unidirectional surface-plasmon–polariton propagation [8,9,13]. We configure our antenna array to have rows of the device matrix **M** correspond to four elliptically polarized states with different helicities and azimuths, as shown in Fig. 2(a). Measurement of these four polarization components unambiguously determines the location of the signal SOP on the Poincaré sphere.

Subwavelength rod antennas emit approximately the field of an electric dipole when electromagnetic radiation polarized parallel to their axis is incident upon them. Many such antennas placed in a row with subwavelength spacing will collectively emit a cylindrical wave when radiation is normally incident on the row and polarized parallel to the constituent antennas (see Supplement 1, Section 1). The waves emitted by two parallel rows of subwavelength antennas with orientation $\pm45°$ with respect to the row axis will interfere to form a radiation field that is asymmetric in the lateral direction [Fig. 2(b)]. The directionality of this radiation field depends on both amplitude and relative phase of the orthogonal linear polarization components that drive each antenna row (see Supplement 1, Section 2).

As special cases, antenna rows spaced by $(m + 1/2)(\lambda/2)$, where m is an integer, will directionally scatter circularly polarized light of different handedness in opposite directions [9], while rows spaced by integer multiples of $\lambda/2$ will maximally scatter light that is linearly polarized along the row axis equally in both directions. For other spacings [in the present configuration, we use a row spacing of $(1 + 1/8)\lambda$], and left- and right-handed *elliptically* polarized light is directionally scattered in opposite directions [Fig. 2(c)]. Two pairs of rows superimposed at a relative angle of $45°$ may then selectively scatter the required four elliptical polarization states shown in Fig. 2(a) in different spatial directions [Fig. 2(d)], as a rotation of the row of antennas by $45°$ with respect to the incident radiation corresponds to a $90°$ rotation of the
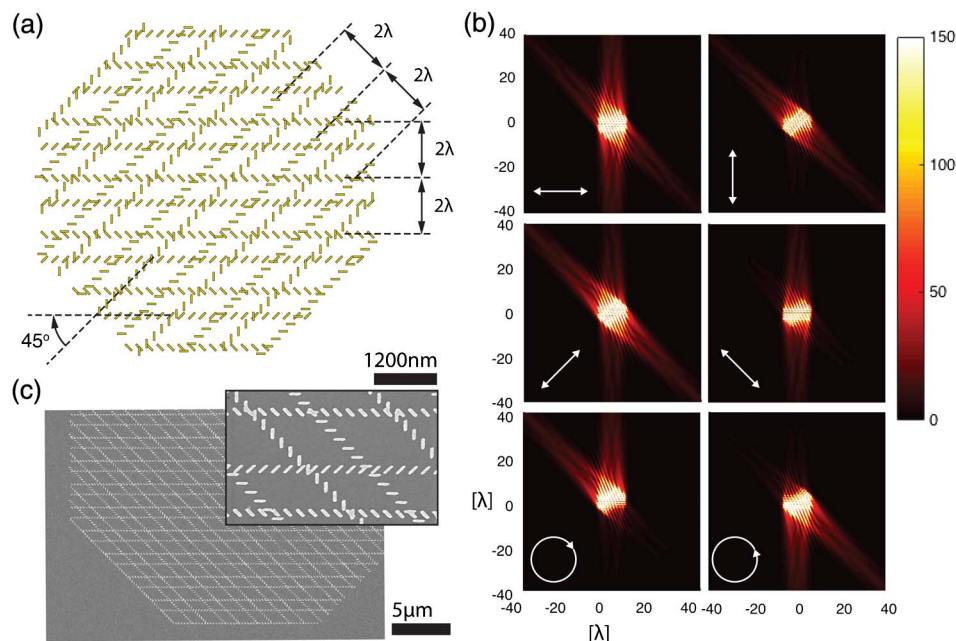
Fig. 3. Polarimetric antenna array. (a) The cross section of the polarimeter is increased by patterning several pairs of antenna rows with a separation of 2λ, resulting in a patch as shown. (b) The calculated in-plane scattered field intensity of a polarimetric antenna array with five pairs of rows under illumination with different polarizations in the independent-dipole approximation (in arbitrary units, with the color scale saturated in the central region). The spatial scale is in units of wavelength. The incident polarization states are shown as white arrows and correspond to the cardinal directions on the Poincaré sphere. Each polarization state results in a unique distribution of intensities over the four beams. (c) Scanning electron micrographs of the fabricated structure, designed for operation at telecommunication wavelengths. Inset: close-up showing individual antennas of the array.

scattered SOP vectors in the equatorial plane of the Poincaré sphere (see Supplement 1, Section 4 for a discussion of device matrix implementation).

The cross section of the structure may be enlarged by repeating the row pairs every 2λ in the manner of a grating, resulting in an array of antennas [Fig. 3(a)]. This has the side effect of modulating the scattered field of the row pairs into grating orders, which, for normally incident light at λ, are co-planar and $\approx 60°$ out-of-plane with the polarimeter (see Supplement 1, Section 3). Figure 3(b) shows the predicted in-plane scattered field of such an array for different incident polarization states, each resulting in a unique intensity distribution. The polarization response of the actually implemented antenna array will deviate due to, for example, internal reflections, wavelength dependence, antenna interactions, and possible geometric deviations from the intended design. This necessitates a standard calibration experiment in which the polarization selectivity of the different channels $P_1 - P_4$ in the actual fabricated device across the range of operating wavelengths is determined precisely (see Supplement 1, Section 5).

3. EXPERIMENT

For the purpose of our experiment, the four beams scattered by the antenna array are sampled using outcoupling gratings situated in-plane at a distance 500 µm from the array and picked up in the far field with an imaging detector. This was done primarily to simplify the laboratory setup. In an actual packaged polarimeter device, however, the intensity measurements are more conveniently carried out directly in the configuration depicted in Fig. 1(c).

We fabricate a polarimeter with four output channels and four corresponding outcoupling gratings on top of a double-side-polished silicon wafer that was spin-coated with a 12 µm thick layer of benzocyclobutene polymer (BCB, $n \approx 1.535$ at 1550 nm). The antenna array and the outcoupling gratings were patterned using electron beam lithography, followed by electron beam deposition of Ti (1 nm) + Au (21 nm) and liftoff [Fig. 3(c)]. The structure was then covered with a second 12 µm layer of BCB polymer by spin coating. The resulting individual antennas had a size of approximately 250 nm × 50 nm. The antenna array was designed for a center operating wavelength of $\lambda = 1550$ nm/ $1.535 = 1010$ nm.

In the experiment, light from a tunable laser source (Tunics Plus) was guided toward our polarimeter using a single-mode optical fiber (SMF28) that was placed in mechanical contact with the BCB surface. The structure was imaged through the silicon wafer using an InGaAs camera, where the light directly transmitted through the polarimeter was blocked to avoid saturating the camera detector. The SOP of the incident light could be changed arbitrarily by straining the optical fiber and simultaneously be monitored by using a commercially available rotating-wave-plate polarimeter (Thorlabs PAX5710IR3-T) using a removable mirror [Fig. 4(a)]. The camera image shows the scattering from the outcoupling gratings as bright spots that change in intensity in response to altering the polarization of the incident light [Fig. 4(b)] (see Supplement 1, Fig. S1). We tested the polarimeter at several wavelengths between 1500 and 1565 nm, covering the C-band telecommunication wavelengths (1530–1565 nm). Calibration measurements were performed for each wavelength to characterize the precise polarization response of the polarimeter, as
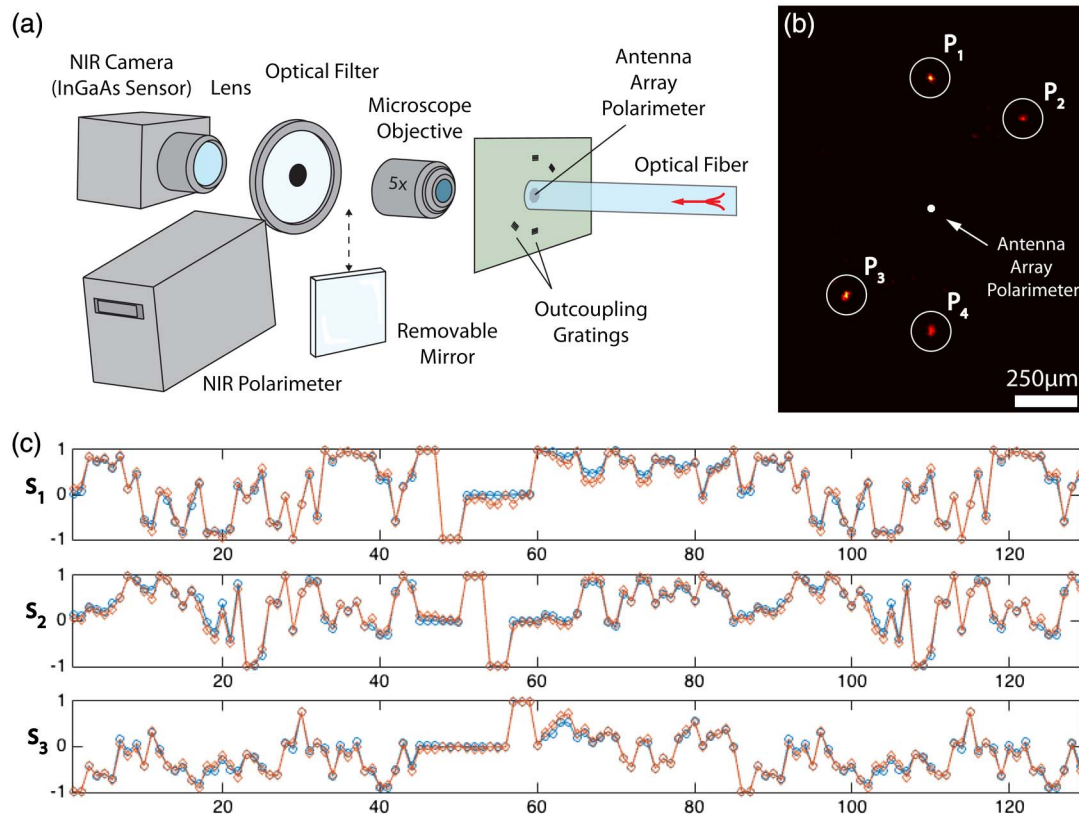
Fig. 4. Experimental implementation of the antenna array polarimeter. (a) Setup for characterizing the antenna array polarimeter. The array is positioned at the end facet of an optical fiber, which carries light from a tunable laser source at telecommunication wavelengths. The state of polarization of the light is modified by straining the fiber and monitored by a commercial NIR polarimeter via a removable mirror. The intensity of the light scattered by the outcoupling grating is measured by imaging them using a NIR camera with an InGaAs sensor, where the light directly transmitted through the metasurface is shadowed with an optical filter. (b) Camera image of the outcoupling gratings, showing polarization-dependent intensities P_1, P_2, P_3, and P_4 scattered by the four outcoupling gratings marked with white circles. The antenna array is shown to scale as a white overlay. (c) Measurement of the state of polarization (s_1, s_2, s_3) of 129 arbitrarily selected polarizations using the commercial polarimeter (blue) and the metasurface polarimeter (orange).

described in Supplement 1, Section 5. A number of independent SOP measurements performed using the antenna array polarimeter and the commercial polarimeter were compared for multiple arbitrary polarizations, representative of all possible SOPs on the Poincaré sphere. The results for measurements for incident light at a wavelength of 1550 nm are given in Fig. 4(c), with similar plots for wavelengths between 1500 and 1565 nm provided in Supplement 1, Figs. S2–S4. In all cases, excellent agreement is observed between the SOP measurements derived from the antenna array and from the rotating-wave-plate polarimeter. Our design is clearly superior, however, in terms of potential compactness, speed, and stability. Fully packaged, the performance of the antenna array polarimeter may well match that of state-of-the-art fiber-based in-line polarimeters, where sampling rates and sensitivities are detector limited, while additionally offering much simpler construction and applicability for free-space radiation as well as other wavelength ranges where detectors are available.

The layout of the antenna array used in the current work was intended primarily for SOP measurements, but also allows for intensity measurements, since fully polarized laser light with unchanging DOP was used. Intensity fluctuations manifest themselves as homogeneous changes in all channel intensities, and corresponding data is provided in Supplement 1, Fig. S5. Furthermore, more complex antenna array designs that enable

DOP measurements are provided, which rely on six or more outputs (which do not all have to be read out). For the present purpose, the simplest possible four-output design was adequate.

4. CONCLUDING REMARKS

In conclusion, we have demonstrated a fundamentally new architecture for practical, nondestructive polarization measurements based on a single 2D array of rod antennas. The concept relies on the detection of polarization-selective directional scattering. By reducing the polarimeter to a single ultracompact optical component and four or more detectors, the proposed architecture can substantially outperform existing polarimeters in terms of size, cost, and complexity. The antenna arrays can furthermore be scaled to operate at most technologically relevant wavelengths, enabling polarimetry in wavelength ranges where it was previously very difficult, such as the mid-IR. Through these improvements, our polarimeter design promises to make in-line polarization measurements accessible to a much broader spectrum of applications with portable mass-produced ultracompact polarimeter devices.

See Supplement 1 for supporting content.

REFERENCES

1. E. Collett, *Polarized Light* (CRC Press, 1993).
2. L. D. Barron, *Molecular Light Scattering and Optical Activity*, 2nd ed. (Cambridge University, 2004).
3. A. Kavokin, J. J. Baumberg, G. Malpuech, and F. P. Laussy, *Microcavities* (Oxford University, 2011).
4. A. Lipson, S. G. Lipson, and H. Lipson, *Optical Physics* (Cambridge University, 2010).
5. W. A. Hiltner, "Polarization of light from distant stars by interstellar medium," Science **109**, 165 (1949).
6. P. A. R. Ade, R. W. Aikin, M. Amiri, D. Barkats, S. J. Benton, C. A. Bischoff, J. J. Bock, J. A. Bonetti, J. A. Brevik, I. Buder, E. Bullock, G. Chattopadhyay, G. Davis, P. K. Day, C. D. Dowell, L. Duband, J. P. Filippini, S. Fliescher, S. R. Golwala, M. Halpern, M. Hasselfield, S. R. Hildebrandt, G. C. Hilton, V. Hristov, H. Hui, K. D. Irwin, W. C. Jones, K. S. Karkare, J. P. Kaufman, B. G. Keating, S. Kefeli, S. A. Kernasovskiy, J. M. Kovac, C. L. Kuo, H. G. LeDuc, E. M. Leitch, N. Llombart, M. Lueker, P. Mason, K. Megerian, L. Moncelsi, C. B. Netterfield, H. T. Nguyen, R. O'Brient, R. W. Ogburn IV, A. Orlando, C. Pryke, A. S. Rahlin, C. D. Reintsema, S. Richter, M. C. Runyan, R. Schwarz, C. D. Sheehy, Z. K. Staniszewski, R. V. Sudiwala, G. P. Teply, J. E. Tolan, A. Trangsrud, R. S. Tucker, A. D. Turner, A. G. Vieregg, A. Weber, D. V. Wiebe, P. Wilson, C. L. Wong, K. W. Yoon, and J. Zmuidzinas, "Antenna-coupled TES bolometers used in BICEP2, Keck array, and SPIDER," arXiv:1502.00619v1 (2015).
7. J. S. Tyo, D. L. Goldstein, D. B. Chenault, and J. A. Shaw, "Review of passive imaging polarimetry for remote sensing applications," Appl. Opt. **45**, 5453–5469 (2006).
8. J. P. B. Mueller, K. Leosson, and F. Capasso, "Polarization-selective coupling to long-range surface plasmon polariton waveguides," Nano Lett. **14**, 5524–5527 (2014).
9. J. Lin, J. P. B. Mueller, Q. Wang, G. Yuan, N. Antoniou, X.-C. Yuan, and F. Capasso, "Polarization-controlled tunable directional coupling of surface plasmon polaritons," Science **340**, 331–334 (2013).
10. J. Petersen, J. Volz, and A. Rauschenbeutel, "Chiral nanophotonic waveguide interface based on spin-orbit interaction of light," Science **346**, 67–71 (2014).
11. S.-Y. Lee, I.-M. Lee, J. Park, S. Oh, W. Lee, K.-Y. Kim, and B. Lee, "Role of magnetic induction currents in nanoslit excitation of surface plasmon polaritons," Phys. Rev. Lett. **108**, 213907 (2012).
12. F. J. Rodríguez-Fortuño, G. Marino, P. Ginzburg, D. O'Connor, A. Martínez, G. A. Wurtz, and A. V. Zayats, "Near-field interference for the unidirectional excitation of electromagnetic guided modes," Science **340**, 328–330 (2013).
13. L. Huang, X. Chen, B. Bai, Q. Tan, G. Jin, T. Zentgraf, and S. Zhang, "Helicity dependent directional surface plasmon polariton excitation using a metasurface with interfacial phase discontinuity," Light Sci. Appl. **2**, e70 (2013).
14. M. Totzeck, W. Ulrich, A. Göhnermeier, and W. Kaiser, "Semiconductor fabrication: pushing deep ultraviolet lithography to its limits," Nat. Photonics **1**, 629–631 (2007).
15. M. R. Shcherbakov, P. P. Vabishchevich, M. I. Dobynde, T. V. Dolgova, A. S. Sigov, C. M. Wang, D. P. Tsai, and A. A. Fedyanin, "Plasmonic enhancement of linear birefringence and linear dichroism in anisotropic optical metamaterials," J. Exp. Theor. Phys. Lett. **90**, 433–437 (2009).
16. M. Anastasiadou, A. D. Martino, and D. Clement, "Polarimetric imaging for the diagnosis of cervical cancer," Phys. Status Solidi C **5**, 1423–1426 (2008).
17. S. Bauer, B. Grees, D. Spitzer, M. Beck, R. Bottesch, H.-W. Ortjohann, B. Ostrick, T. Schäfer, H. H. Telle, A. Wegmann, M. Zbořil, and C. Weinheimer, "Ellipsometry with polarisation analysis at cryogenic temperatures inside a vacuum chamber," arXiv:1307.5879v1 (2013).
18. M. Neshat and N. P. Armitage, "Developments in THz range ellipsometry," arXiv:1305.3127v1 (2013).
19. J. N. Damask, *Polarization Optics in Telecommunications* (Springer, 2004).
20. G. P. Agrawal, *Fiber-Optic Communication Systems* (Wiley, 2012).
21. A. Ling, S. K. Pang, A. Lamas-Linares, and C. Kurtsiefer, "An optimal photon counting polarimeter," J. Mod. Opt. **53**, 1523–1528 (2006).
22. H. Hübel, M. R. Vanner, T. Lederer, B. Blauensteiner, T. Lorünser, A. Poppe, and A. Zeilinger, "High-fidelity transmission of polarization encoded qubits from an entangled source over 100 km of fiber," Opt. Express **15**, 7853–7862 (2007).
23. H. J. Kimble, "The quantum Internet," Nature **453**, 1023–1030 (2008).
24. A. Peinado, "Design of polarimeters based on liquid crystals and biaxial crystals for polarization metrology," Tesis Doctorals en Xarxa (Universitat Autònoma de Barcelona, 2014), http://tdx.cbuc.es/handle/10803/285054.
25. N. Yu, P. Genevet, M. A. Kats, F. Aieta, and J. P. Tetienne, "Light propagation with phase discontinuities: generalized laws of reflection and refraction," Science **334**, 333–337 (2011).
26. F. Aieta, M. A. Kats, P. Genevet, and F. Capasso, "Multiwavelength achromatic metasurfaces by dispersive phase compensation," Science **347**, 1342–1345 (2015).
27. F. Aieta, P. Genevet, M. A. Kats, N. Yu, and R. Blanchard, "Aberration-free ultrathin flat lenses and axicons at telecom wavelengths based on plasmonic metasurfaces," Nano Lett. **12**, 4932–4936 (2012).
28. N. Yu, F. Aieta, P. Genevet, M. A. Kats, and Z. Gaburro, "A broadband, background-free quarter-wave plate based on plasmonic metasurfaces," Nano Lett. **12**, 6328–6333 (2012).
29. F. Afshinmanesh, J. S. White, W. Cai, and M. L. Brongersma, "Measurement of the polarization state of light using an integrated plasmonic polarimeter," Nanophotonics **1**, 125–129 (2012).
30. J. J. Peltzer and K. A. Bachman, "Plasmonic micropolarizers for full Stokes vector imaging," Proc SPIE **8364**, 83640O (2012).
31. F. Gori, "Measuring Stokes parameters by means of a polarization grating," Opt. Lett. **24**, 584–586 (1999).
32. Z. Bomzon, G. Biener, V. Kleiner, and E. Hasman, "Spatial Fourier-transform polarimetry using space-variant subwavelength metal-stripe polarizers," Opt. Lett. **26**, 1711–1713 (2001).
33. E. Laux, C. Genet, T. Skauli, and T. W. Ebbesen, "Plasmonic photon sorters for spectral and polarimetric imaging," Nat Photonics **2**, 161–164 (2008).
34. I. Mandel, J. N. Gollub, I. Bendoym, and D. T. Crouse, "Theory and design of a novel integrated polarimetric sensor utilizing a light sorting metamaterial grating," IEEE Sens. J. **13**, 618–625 (2013).
35. A. Pors, M. G. Nielsen, and S. I. Bozhevolnyi, "Plasmonic metagratings for simultaneous determination of Stokes parameters," Optica **2**, 716–723 (2015).
36. D. Wen, F. Yue, Y. Ma, M. Chen, X. Ren, P. E. Kremer, B. D. Gerardot, M. R. Taghizadeh, G. S. Buller, and X. Chen, "Metasurface for characterization of the polarization state of light," Opt. Express **23**, 10272–10281 (2015).
37. R. M. A. Azzam, "In-line light-saving photopolarimeter and its fiber-optic analog," Opt. Lett. **12**, 558–560 (1987).
38. S. Huard, *Polarization of Light* (Wiley, 1997).
39. J. S. Tyo, "Design of optimal polarimeters: maximization of signal-to-noise ratio and minimization of systematic error," Appl. Opt. **41**, 619–630 (2002).